FGF22 signaling regulates synapse formation during post-injury remodeling of the spinal cord

Anne Jacobi[1], Kristina Loy[1], Anja M. Schmalz[1], Mikael Hellsten[1], Hisashi Umemori[2,3], Martin Kerschensteiner[1,4] and Florence M. Bareyre[1,4]

Supplementary Figure Legends

Figure S1. Hindlimb CST maturation is not altered in FGF22 deficient mice.

A Confocal images of the cortex of an adult FGF22 competent mouse. Scale bar equals 100 µm.

B Confocal images of the cortex of an adult FGF22 deficient mouse. Scale bar equals 100 µm.

C Quantification of the number of neurons in an area of 37.5mm^2 of layer V of the motor and somatosensory cortex in adult FGF22 competent and FGF22 deficient mice (n=3 animals per group). Mean±SEM. No significant differences between the groups were detected (unpaired two-tailed t-test).

D Quantification of the number of boutons per µm hindlimb CST collateral in the cervical and lumbar spinal cord of adult FGF22 competent and deficient mice (n=6 animals per group). Mean±SEM. No significant differences between the groups were detected (unpaired two-tailed t-test).

E Quantification of the number of branchpoints per µm hindlimb CST collateral in the cervical and lumbar spinal cord of adult FGF22 competent and deficient mice (n=6

animals per group). Mean±SEM. No significant differences between the groups were detected (unpaired two-tailed t-test).

F Quantification of the number of exiting hindlimb CST collaterals in the cervical and lumbar spinal cord of adult FGF22 competent and deficient mice (n=6 animals per group). Mean±SEM. No significant differences between the groups were detected (unpaired two-tailed t-test).

Figure S2. Quantification of the average length of the collaterals in control, FGF22 deficient and FGFR deficient mice.

A Quantification of average collateral length in FGF competent (white bar) and FGF22 deficient (red bar) mice.

B Quantification of average collateral length in FGF competent (white bar) and FGFR1 forebrain deficient (dark blue bar) and forebrain FGFR2 deficient (dark green bar) mice.

C Quantification of average collateral length in FGF competent (white bar) and FGFR1R2 hindlimb motor cortex co-deficient (light blue bar) mice.

Figure S3. Hindlimb CST maturation is not altered in forebrain FGFR1 deficient mice.

A Confocal images of the cortex of an adult FGFR competent mouse. Scale bar equals 100 µm.

B Confocal images of the cortex of an adult, forebrain FGFR1 deficient mouse. Scale bar equals 100 µm.

C Quantification of the number of neurons in an area of 37.5mm^2 of layer V of the motor and somatosensory cortex in adult FGFR competent and FGFR1 deficient mice (n=3 animals per group). Mean±SEM. No significant differences between the groups were detected (unpaired two-tailed t-test).

D Quantification of the number of boutons per µm hindlimb CST collateral in the cervical and lumbar spinal cord of adult FGFR competent and FGFR1 deficient mice (n=4 animals per group). Mean±SEM. No significant differences between the groups were detected (unpaired two-tailed t-test).

E Quantification of the number of branchpoints per µm hindlimb CST collateral in the cervical and lumbar spinal cord of adult FGFR competent and FGFR1 deficient mice (n=4 animals per group). Mean±SEM. No significant differences between the groups were detected (unpaired two-tailed t-test).

F Quantification of the number of exiting hindlimb CST collaterals in the cervical and lumbar spinal cord of adult FGFR competent and FGFR1 deficient mice (n=4 animals per group). Mean±SEM. No significant differences between the groups were detected (unpaired two-tailed t-test).

Figure S4. Hindlimb CST maturation is not altered in forebrain FGFR2 deficient mice.

A Confocal images of the cortex of an adult FGFR competent mouse. Scale bar equals 100 µm.

B Confocal images of the cortex of an adult, forebrain FGFR2 deficient mouse. Scale bar equals 100 µm.

C Quantification of the number of neurons in an area of 37.5mm^2 of layer V of the motor and somatosensory cortex in adult FGFR competent and FGFR2 deficient mice (n=3 animals per group). Mean±SEM. No significant differences between the groups were detected (unpaired two-tailed t-test).

D Quantification of the number of boutons per µm hindlimb CST collateral in the cervical and lumbar spinal cord of adult FGFR competent and FGFR2 deficient mice (n=7-8 animals per group). Mean±SEM. No significant differences between the groups were detected (unpaired two-tailed t-test).

E Quantification of the number of branchpoints per µm hindlimb CST collateral in the cervical and lumbar spinal cord of adult FGFR competent and FGFR2 deficient mice (n=7-8 animals per group). Mean±SEM. No significant differences between the groups were detected (unpaired two-tailed t-test).

F Quantification of the number of exiting hindlimb CST collaterals in the cervical and lumbar spinal cord of adult FGFR competent and FGFR2 deficient mice (n=7-8 animals per group). Mean±SEM. No significant differences between the groups were detected (unpaired two-tailed t-test).

Figure S5. Deletion of either FGFR1 or FGFR2 alone does not affect functional recovery after spinal cord injury.

A Quantification of functional recovery in the ladder rung test (irregular walk) in control (white bars) and forebrain FGFR1 (blue bars) or FGFR2 (green bars) deficient mice (n=8-14 mice per group). Mean±SEM. No significant differences between the groups were detected (repeated-measure ANOVA followed by Bonferroni tests).

B Quantification of functional recovery in the ladder rung test (regular walk) in control (white bars) and forebrain FGFR1 (blue bars) or FGFR2 (green bars) deficient mice (n=8-14 mice per group). Mean±SEM. No significant differences between the groups were detected (repeated-measure ANOVA followed by Bonferroni tests).

Figure S6. FGFR2 is located in CST collaterals and in particular in CST boutons.

A Confocal image of FGFR2 immunoreactivity in the cortex of an FGFR competent (left panel) and an FGFR2 deficient mouse (right panel). The inset on the left panel is a magnification of the boxed area. Scale bar equals 100μm in **A** and 10μm in inset.

B Single confocal image plane of FGFR2 immunoreactivity in the corticospinal tract imaged on a cross section of the cervical spinal cord 3weeks following lesioned in FGFR competent mouse (FGFR2: green; CST: red). The boxed area in B is magnified 2 times in the right panels which show the overlay and the single channels. Scale bar equals 10 μm.

C Single confocal plane of FGFR2 immunoreactivity in and around a CST collateral imaged on a cross section in the cervical gray matter (FGFR2: green; CST collateral: red). The boxed area in C is magnified 2 times in the right panels, which show the overlay and the single channels. Scale bar equals 10 μm.

Figure S7. Stereotactic injection of AAVs allows selective targeting of the hindlimb motor cortex.

A Confocal image of the hindlimb motor cortex 3 weeks following injection of a rAAV-GFP-Ires-Cre illustrating the presence of many transduced neurons (green) in layer V of the cortex (blue, counterstaining with Neurotrace 435/455). Scale bar equals 150 μm.

B No transduced neurons (green) are seen in the forelimb motor cortex of the same animal. Same scale as **A**.

Figure S8. Viral and genetic deletion of FGFR2 have similar effects on post-injury remodeling.

A Confocal images of hindlimb CST collaterals exiting the main CST tract (arrows) in the cervical spinal cord 3 weeks following a T8 dorsal bilateral hemisection in FGFR2 floxed mice after injection of either rAAV-GFP (left panel) or rAAV-GFP-Ires-Cre (right panel) in the hindlimb motor cortex. Scale bar equals in 40 μm.

B Quantification of the number of exiting hindlimb CST collaterals in the cervical spinal cord 3 weeks following spinal cord injury in FGFR2 floxed mice after injection of either rAAV-GFP or rAAV-GFP-Ires-Cre in the hindlimb motor cortex (n=7-8 animals per group). The observed increase of CST sprouting is similar to the one observed after stable genetic deletion of FGFR2 (cf. **Fig 4C**). Mean±SEM. ** P =0.004 (unpaired two-tailed t-test).

C Confocal images showing putative synaptic boutons (arrows) on newly formed cervical hindlimb CST collaterals 3 weeks following spinal cord injury in FGFR2 floxed mice after injection of either rAAV-GFP (left panel) or rAAV-GFP-Ires-Cre (right panel) in the hindlimb motor cortex. Scale bar equals in 15 μm.

D Quantification of the number of boutons on cervical CST collaterals at 3 weeks after injury in FGFR2 floxed mice after injection of either rAAV-GFP or rAAV-GFP-Ires-Cre in the hindlimb motor cortex (n=7-8 animals per group). The changes are similar to those obtained by stable genetic deletion of FGFR2 (cf **Fig 4E**). Mean±SEM. * *P* =0.04 (unpaired two-tailed t-test).

E Quantification of the percentage of LPSN contacted by cervical CST collaterals at 3 weeks after injury in FGFR2 floxed mice after injection of either rAAV-GFP or rAAV-GFP-Ires-Cre in the hindlimb motor cortex (n=7-8 animals per group). Again the results are similar to those obtained by stable genetic deletion of FGFR2 (cf **Fig 4F**). Mean±SEM. No significant differences were found (unpaired two-tailed t-test).

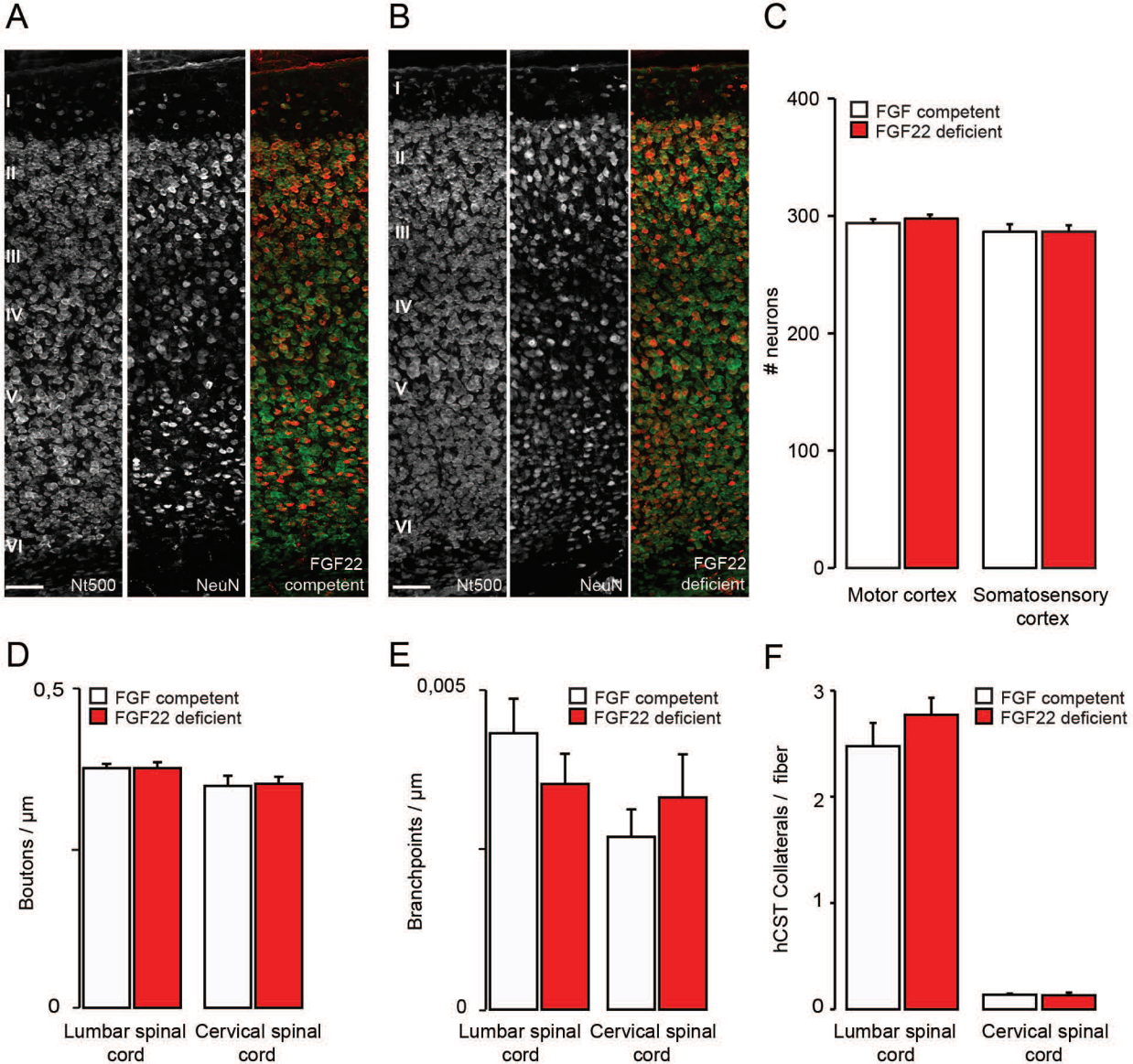

Jacobi et al., Figure S1

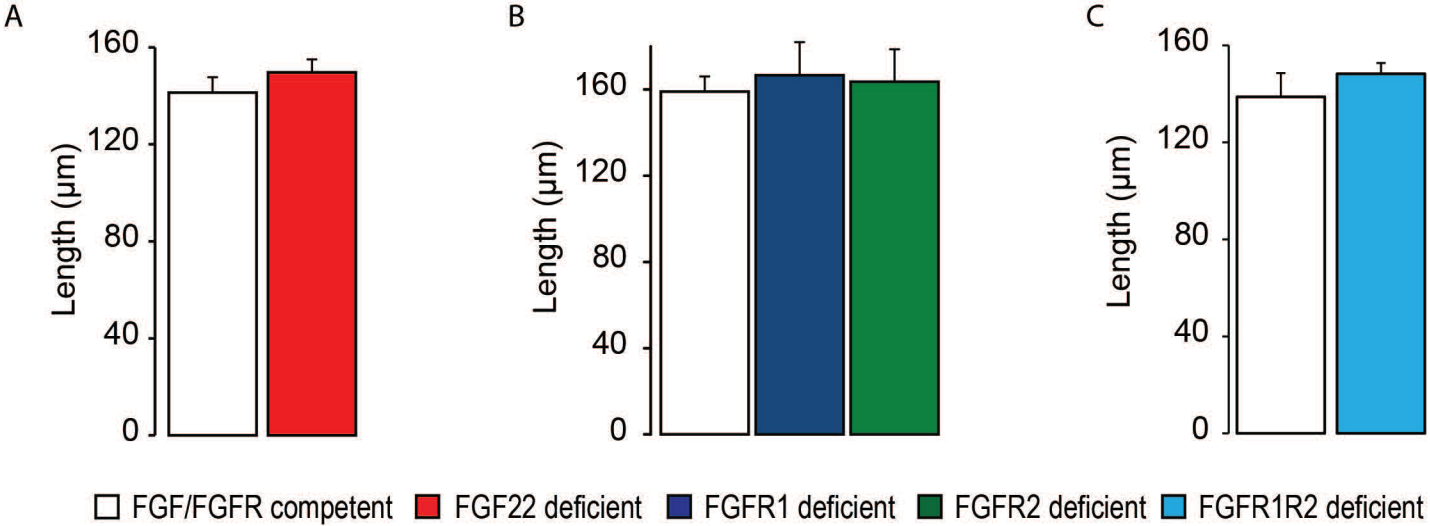

Jacobi et al., Figure S2

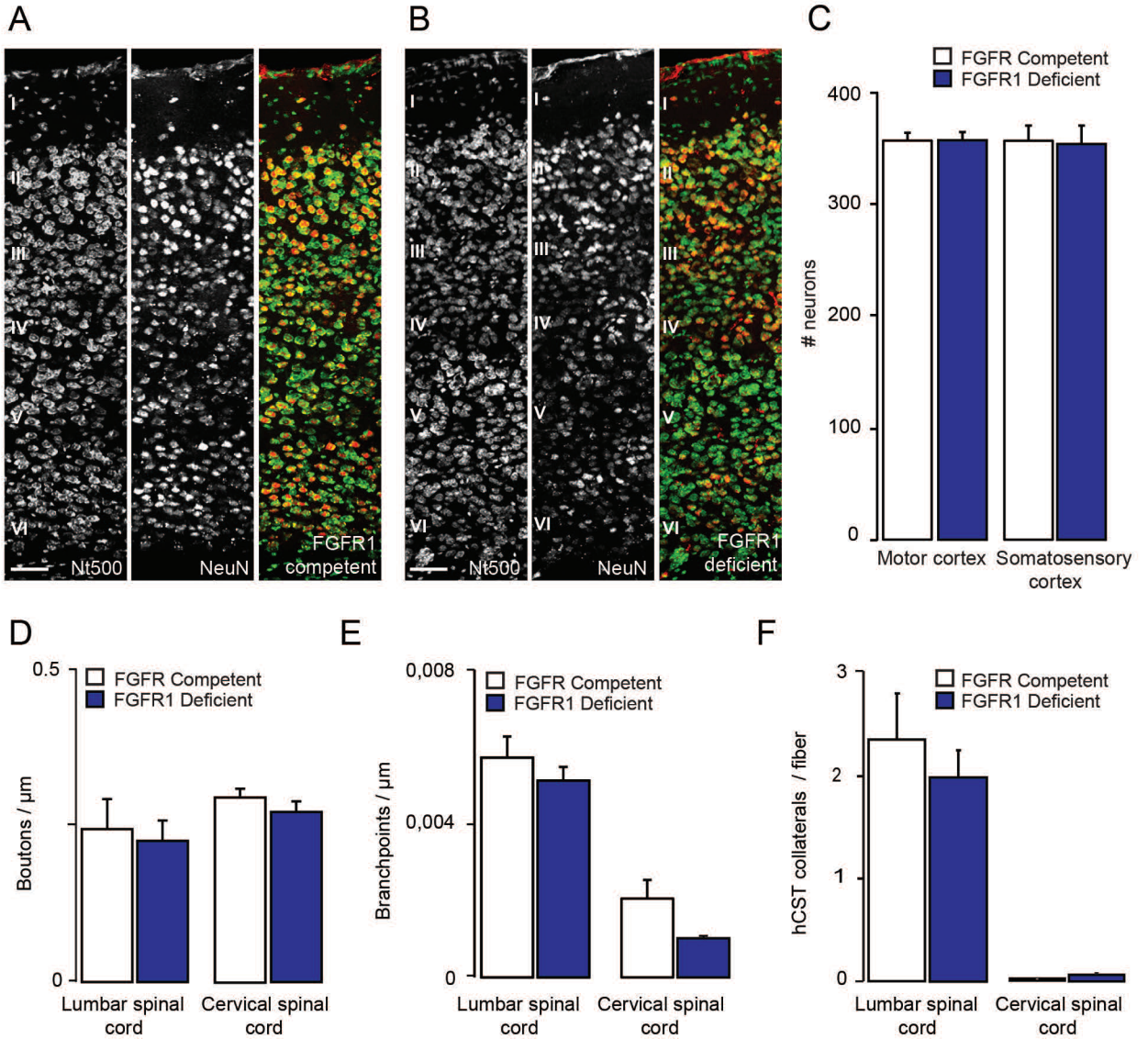

Jacobi et al., Figure S3

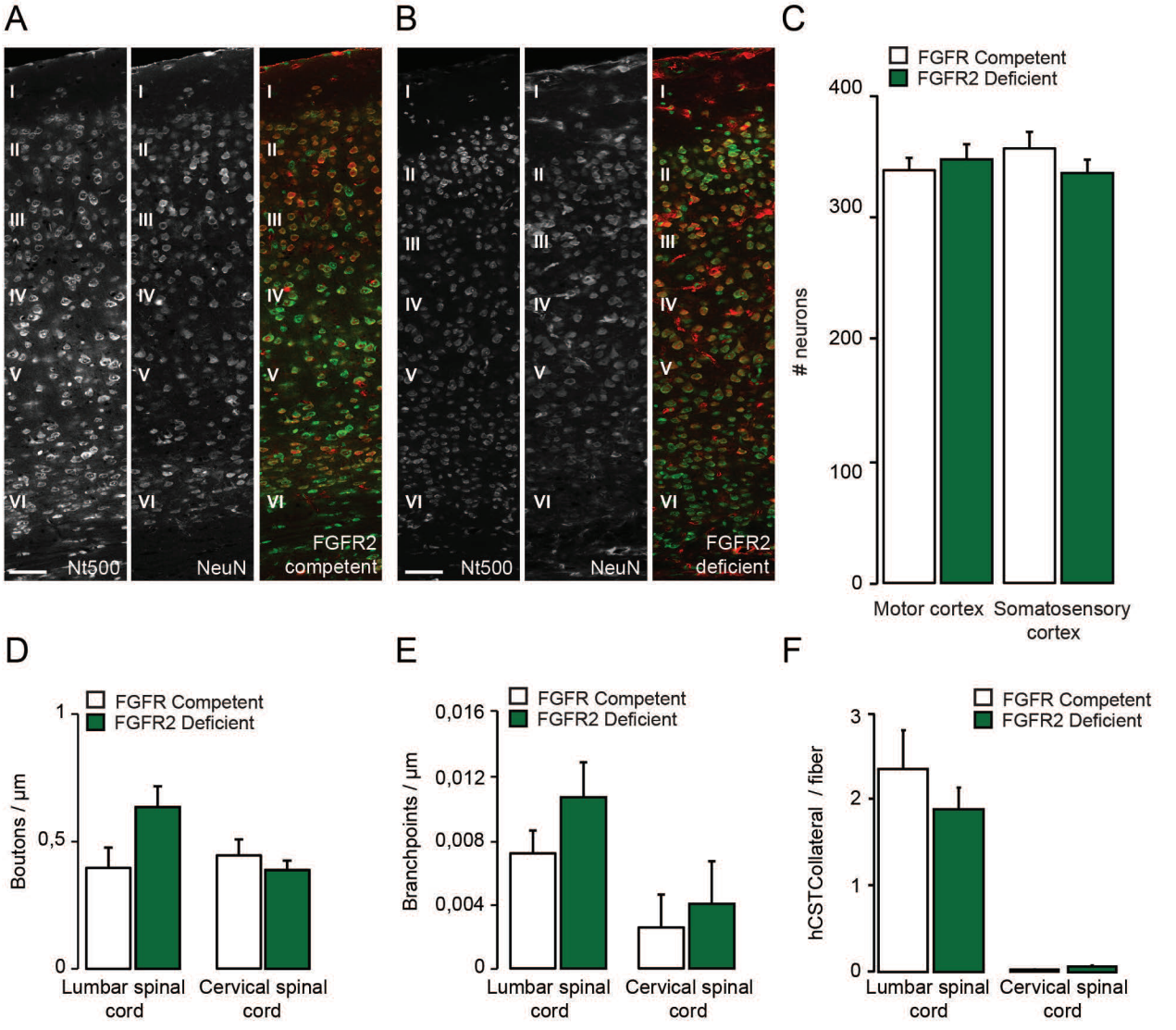

Jacobi et al., Figure S4

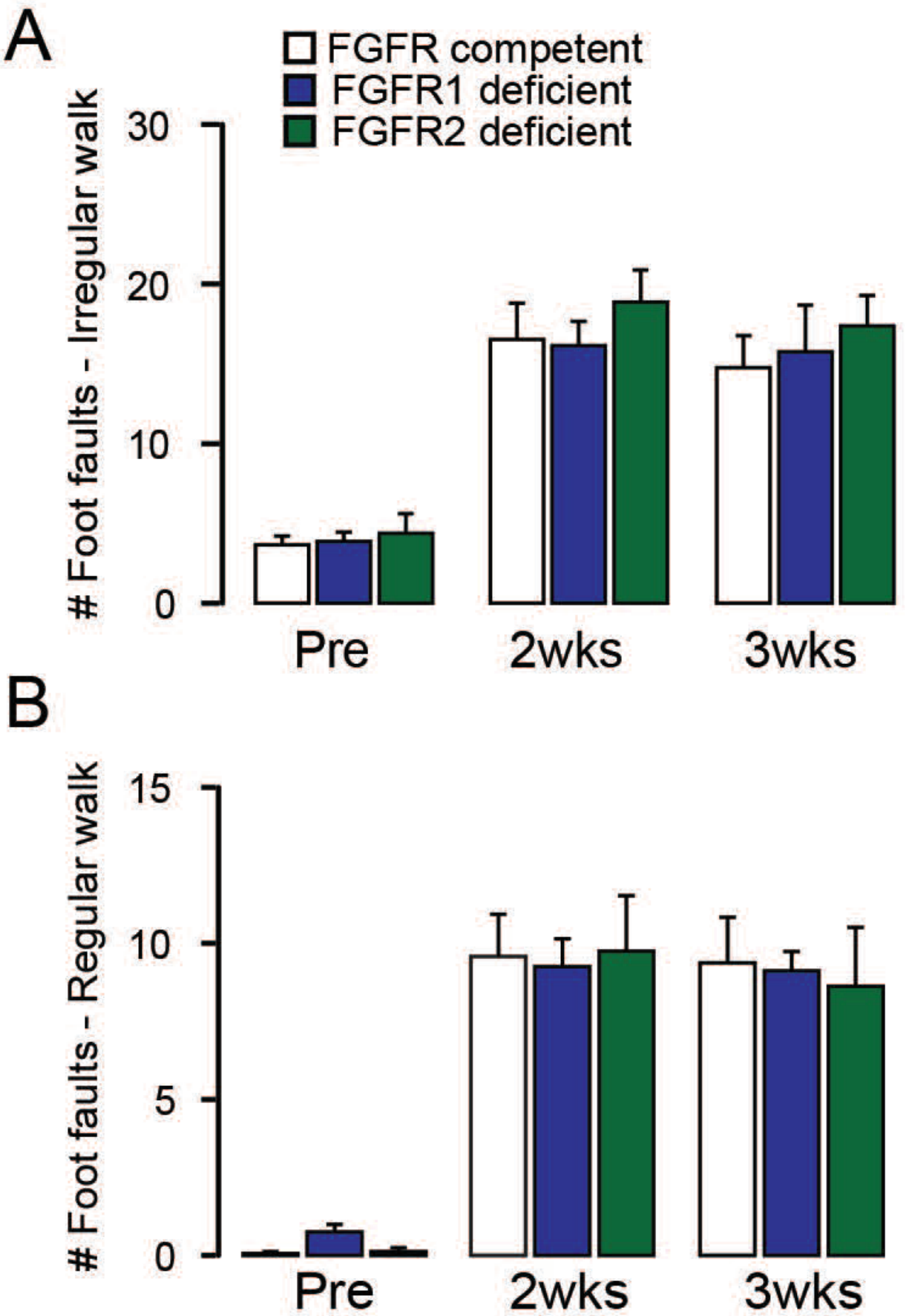

Jacobi et al., Figure S5

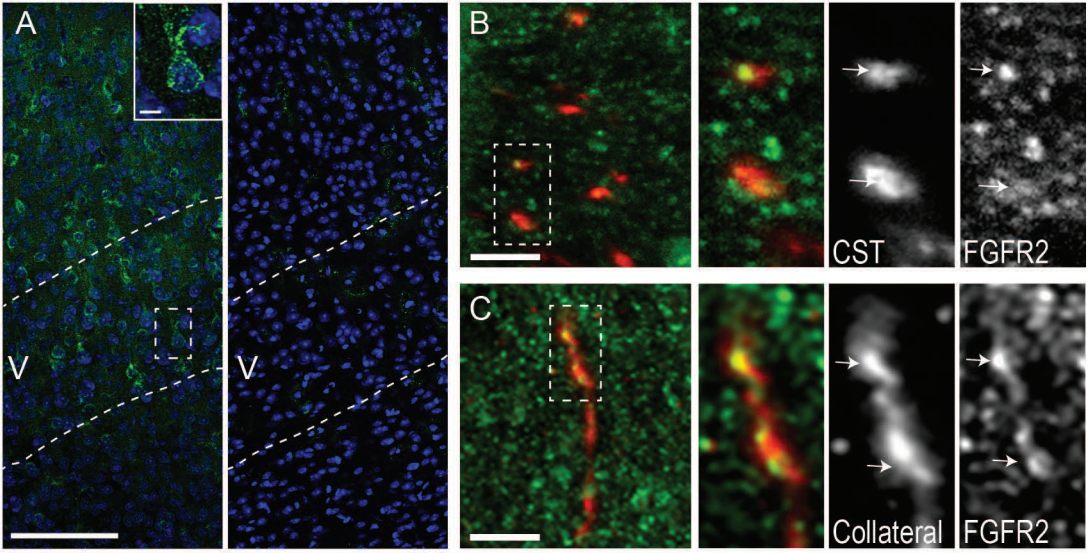

Jacobi et al., Figure S6

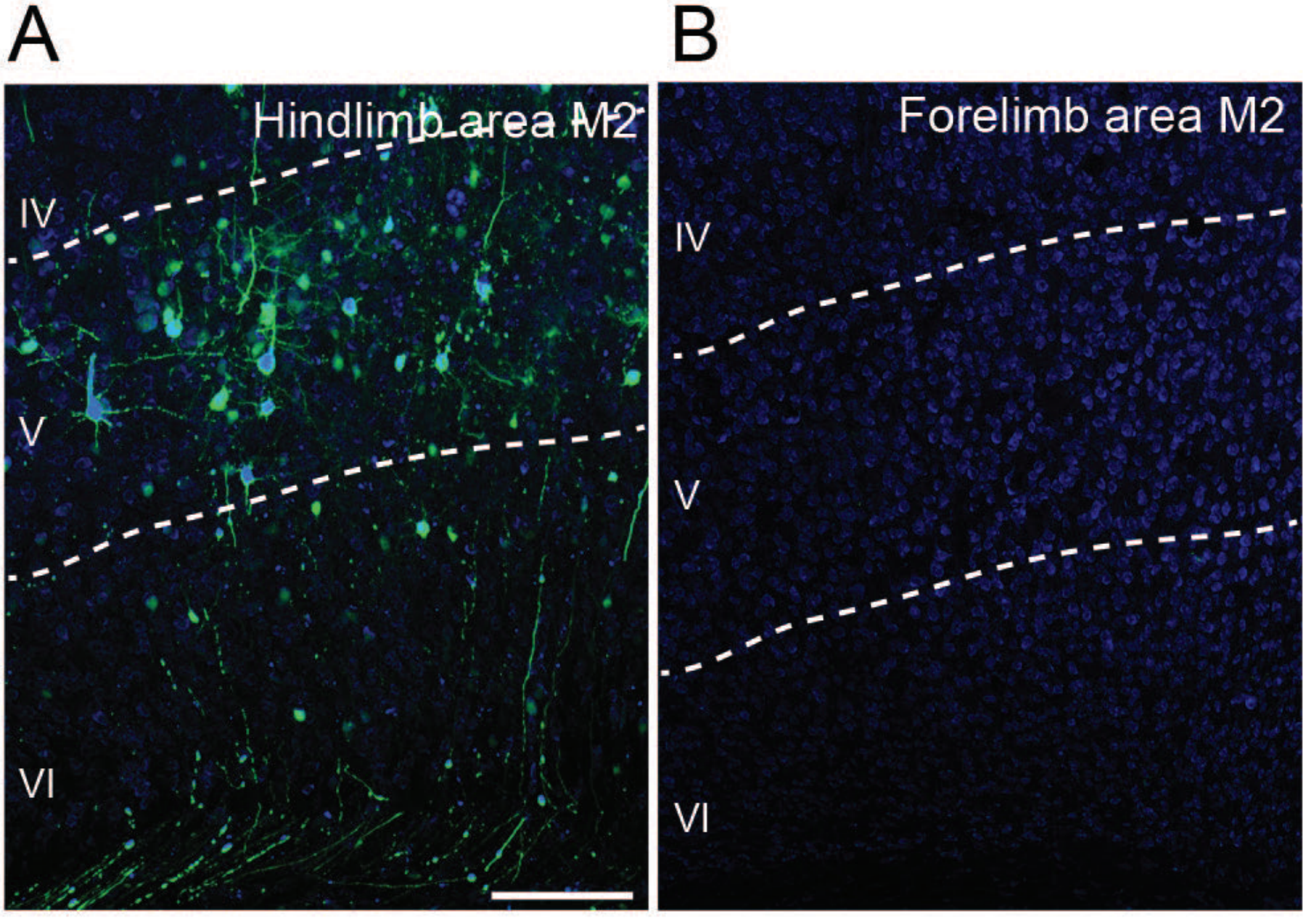

Jacobi et al., Figure S7

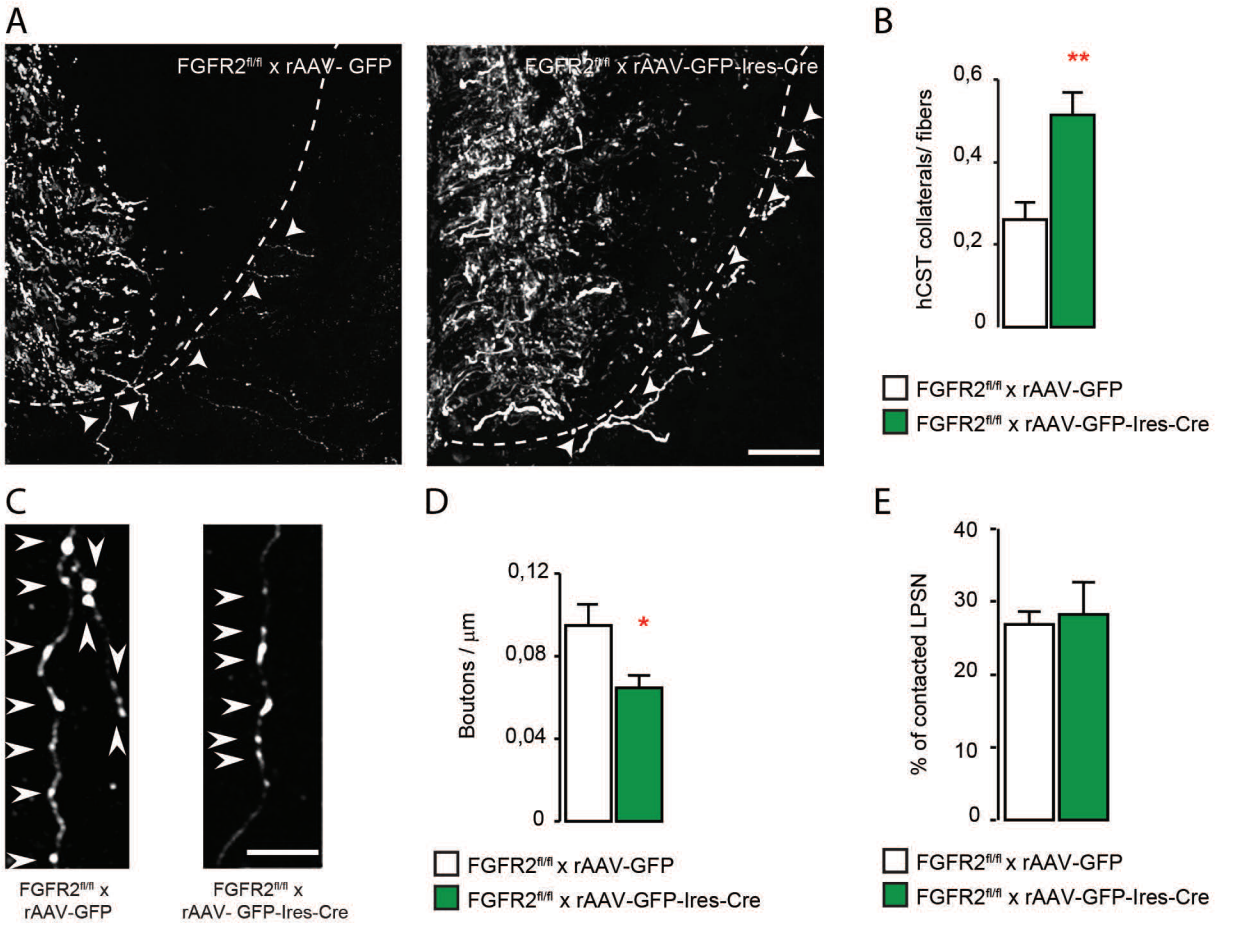

Jacobi et al., Figure S8